Influence of Electron Collisions Inside the Cathode Sheath Upon the Electron Energy Spectrum in the Negative Glow Region of a Gas Discharge

B. SHI, G. J. FETZER, Z. YU, J. D. MEYER, AND G. J. COLLINS, FELLOW, IEEE

Abstract—**Computer models have been developed to solve the Boltzmann equation for the electron energy spectrum in both the cathode sheath and the negative glow region of a glow discharge. Electron collisions occurring during acceleration inside the cathode sheath partially determine the structure of the electron energy distribution measured in the negative glow. The relative role of elastic, excitation, and ionization collisions are examined using the computer model. Good qualitative agreement was obtained between calculated electron energy distributions and previous experimental measurements both at the sheath–plasma interface as well as in the negative glow region of the discharge.**

I. Introduction

THE electron energy distribution in the negative glow region of a glow discharge is considered favorable for the excitation and ionization of atoms primarily because the energy distribution possesses a significant number of high-energy electrons compared to the positive column region of the discharge. Gill and Well [1] measured the energy spectrum of the electron flux $I(E)$ at the boundary of the sheath and negative glow regions of a planar electrode glow discharge for helium pressures of 3–25 torr in order to stimulate hollow cathode discharge conditions. Gill and Webb's experimentally measured electron energy distribution data is reproduced in Fig. 1 of this paper. The spectrum can be divided into three energy regions. There is a high-energy beam component at the full cathode fall energy eV_c. Below this, an empty gap is seen in the spectrum approximately 20 eV wide, following which there occurs a secondary peak. Finally, at lower energies, there is a third high-density feature which is characteristic of low-energy electron-beam-pumped glow discharges.

Manuscript received March 21, 1988; revised December 16, 1988. This work was supported by the National Science Foundation, Quantum Electronics Waves and Beams (ECS-8815051, Dr. L. Goldberg) and the Naval Research Laboratory.

B. Shi was with the Department of Electrical Engineering, Colorado State University, Fort Collins, CO 80523. He is now with the Department of Physics, Tsinghua University, Beijing, China.

G. J. Fetzer was with the Department of Electrical Engineering, Colorado State University, Fort Collins, CO 80523. He is now with the OPHIR Corporation, Lakewood, CO 80235.

Z. Yu and G. J. Collins are with the Department of Electrical Engineering, Colorado State University, Fort Collins, CO 80523.

J. D. Meyer was with the Department of Electrical Engineering, Colorado State University, Fort Collins, CO 80523. He is now with the Applied Electron Corporation, Santa Clara, CA 95054.

IEEE Log Number 8926843.

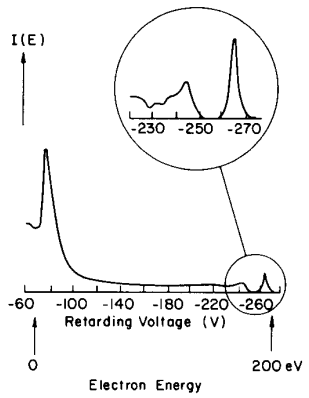

Fig. 1. The electron energy distribution at a sheath–negative glow interface. Adapted from Gill and Webb [1].

In a hollow cathode discharge, the cathode sheath dimension is small, typically 1 mm at a helium pressure of 10 torr [2]. A large portion of the discharge voltage is dropped across the sheath so that a strong electrical field $\vec{E}(\vec{r})$ is a characteristic of the cathode sheath region. Moreover, the steady-state energy distribution of sheath electrons is spatially dependent because of the varying sheath electric field. Hence, a spatially dependent Boltzmann equation must be used in calculations regarding the sheath region. One prior theoretical approach has been to neglect electron–atom collisions occurring inside the cathode sheath [3], [4]. The resultant electron energy distribution function obtained at the cathode sheath-negative glow boundary is a delta function at an energy eV_c corresponding to the discharge voltage drop V_c. The delta function assumption yields a sharp peak in the high-energy region of the theoretical spectrum which does not coincide with the smooth peak of the experimental spectrum shown in Fig. 1.

The primary goal of this theoretical work is to elucidate the relative effects of various electron–atom collision mechanisms on the energy spectrum of electrons being injected from the sheath into the negative glow region of the discharge. In a prior theoretical work, Davis and Vanderslice [5] have constructed a model of the cathode fall region, but only to calculate the energy spectrum of ions impinging on the cathode; they have included only ion

collisions in the sheath and have not considered the evolution of the electron energy distribution through the sheath. In this work, we have developed a numerical model describing the evolution of the electron energy distribution inside the cathode sheath. We also solve a spatially homogeneous steady-state Boltzmann equation in the negative glow for the electron density energy spectrum $N(E)$ at the sheath–bulk plasma interface. Note that the conventional relationship between $N(E)$ and the electron flux density energy spectrum $\vec{I}$ is

$$\vec{I}(E) = N(E)\vec{v} \tag{1}$$

where $\vec{v}$ is the velocity of electrons.

We outline our model assumptions in Section II. Section III deals with the methodology for performing the energy distribution calculations in the sheath region of the plasma. Bulk plasma calculations are discussed in Section IV. Section V contains the results of simulating a glow discharge in helium. Our theoretical results illustrate the relative effects of the various collision mechanisms on the electron energy distribution. Also included in Section V is a comparison of our calculations to the measurements of Gill and Webb at the sheath–glow interface and to the results of Olson and Nordlund [6] inside the negative glow region. Section VI contains a summary of conclusions resulting from this work.

II. The Model

We employ a numerical solution of the Boltzmann equation to obtain the energy spectrum of both the electron flux density in the cathode sheath as well as the electron density in the negative glow. The appropriate form of the Boltzmann equation for both of these conditions is given by

$$\vec{v} \cdot \nabla_r N(\vec{r}, \vec{v}) + \vec{a} \cdot \nabla_v N(\vec{r}, \vec{V}) + \frac{\partial N(\vec{r}, \vec{v})}{\partial t} = \left(\frac{\delta N(\vec{r}, \vec{v})}{\delta t}\right)_c. \tag{2}$$

Here, $N(\vec{r}, \vec{v})$ is the electron density energy distribution function. ∇_r and ∇_v are gradient operators in six-dimensional phase space. $(\delta N(\vec{r}, \vec{v})/\delta t)_c$ is the rate of change of N due to electron–atom and electron–electron collisions. $\vec{a}$ is the acceleration of electrons in the electrical field $\vec{E}$. Because $\partial N/\partial t = 0$ for steady-state conditions, (2) becomes

$$\vec{v} \cdot \nabla_r N(\vec{r}, \vec{v}) + \vec{a} \cdot \nabla_v(\vec{r}, \vec{v}) = \left(\frac{\delta N(\vec{r}, \vec{v})}{\delta t}\right)_c. \tag{3}$$

We have included both elastic and inelastic electron–atom collision mechanisms in our discharge model. The collision mechanisms included are ionization, recombination, excitation, superelastic deexcitation, and momentum transfer collisions. Fig. 2 is a partial energy diagram

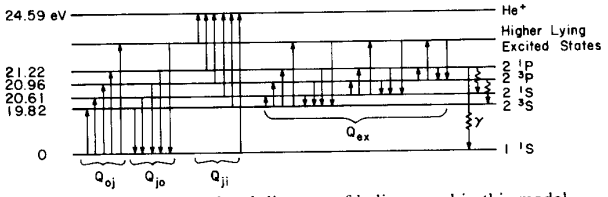

Fig. 2. Partial energy level diagram of helium used in this model.

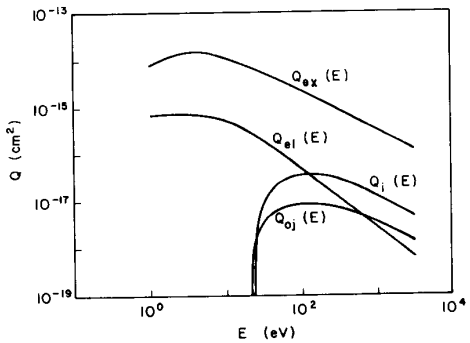

Fig. 3. Comparison of the individual cross sections describing electron–He I collisions versus energy [8], [10]. Q_{el}: elastic cross section, Q_i: ionization cross section, Q_{oj}: groundexcited state cross section, Q_{ex}: excited–excited state cross section.

of the simplified seven-level model of the helium atom and some of the excitation and decay processes considered. Fig. 3 is a plot of the individual electron–neutral collision cross sections for the mechanisms considered. Q_{ex} represents the collision cross section for electron impact excitation from one excited state to another. Although Q_{ex} has the largest value of all cross sections in Fig. 3, the density of excited states is small compared to the density of ground state atoms, and therefore such processes are negligible and have been neglected in our model [7]. We treat the first four excited states of helium individually, but treat higher lying helium with one equivalent level. Elastic collisions dominate at electron energies less than ionization and excitation threshold energies. Ionization and excitation collisions dominate the electron energy transfer for electron energies above 100 eV, with ionization collisions playing the largest role. The electron–helium cross sections we employ mainly come from a database developed at Princeton [8].

Fig. 4 illustrates the various spatial regions of the glow discharge considered in this work, as well as the linear spatial variation of the electric field versus distance in the z direction assumed in the sheath. The assumed functional form of the electric field is in agreement with previous experimental results [9]. The discharge is assumed to be spatially uniform in the x and y directions.

III. Calculations Inside the Sheath Region

We have simplified (3) to a one-dimensional z-dependent Boltzmann equation to determine the electron energy spectrum in the cathode sheath [10]. We assume that the electron velocity component that deviates from

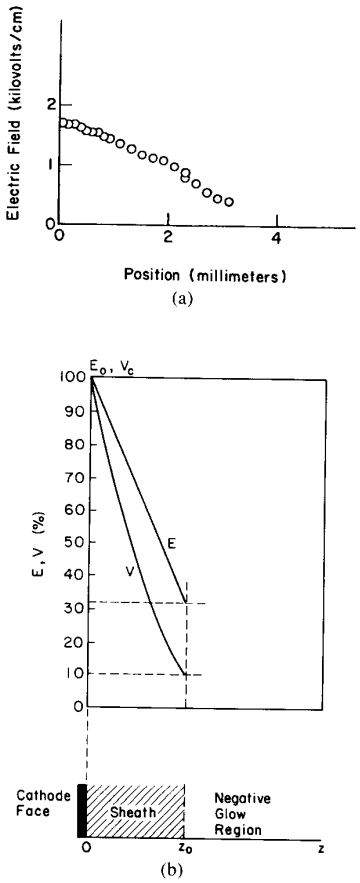

Fig. 4. (a) Measured electric in the cathode sheath by laser optogalvanic study at 1 torr ambient pressure of helium and 0.35 kV discharge voltage. (b) Relative linear electric field E and associated potential V inside the cathode sheath versus relative position. The position z_0 is defined as that location where V drops to $0.1V_c$ and E drops to $E_0/3$.

the z direction is small compared to the velocity it will gain from the z-directed electric field before its next collision. This assumption is reasonable because of the very strong z-directed electrical field in the sheath and because the majority of electrons experience small angle scattering following elastic and inelastic collisions [11]. Low-energy electrons with velocities nonparallel to the z direction will gain energy only from the z-directed electric field. Therefore, these electrons are rapidly redirected with velocities essentially parallel to the sheath field in the z direction. Secondary electrons ejected from ionized neutrals are distributed isotropically [12] and are most likely to be emitted at zero energy [13]. Such electrons will be subsequently accelerated by the strong sheath field to energies in excess of several electron volts before traveling along the z direction more than several hundred microns. We recognize that there will be some loss of electrons from the beam resulting from isotropically emitted electrons near the edge of the sheath towards the negative glow region which are not redirected by the remaining electrical field. The fraction is judged to be small, having little effect on the final results.

According to our laser-optogalvanic study of the electric field distribution in cathode sheath, shown in Fig. 4(a) [9], in this model a linear electric field was used within the cathode sheath. The boundary of the cathode sheath and negative glow is defined as the position z_0 where the voltage drop to 10 percent of the cathode voltage V_c was assumed arbitrary [14]. Clearly, this occurs at different absolute positions under varying experimental conditions. In the linear field model of Fig. 4, the electrical field has a value of $1/3$ of E_0 at the sheath–negative glow interface where E_0 is the maximum electric field strength. Under these assumptions,

$$a_z = \frac{eE}{m}, \quad a_x = 0, \quad a_y = 0,$$

and

$$\frac{\partial N}{\partial x} = 0, \quad \frac{\partial N}{\partial y} = 0$$

(3) becomes

$$v_z \frac{\partial N}{\partial z} + \frac{eE}{m} \frac{\partial N}{\partial v_z} = \left(\frac{\delta N}{\delta t}\right)_c \tag{4}$$

where the collision term $(\delta N/\delta t)_c$ was explicitly described in [10].

Our theoretical calculation starts with a group of electrons emitted from the surface of the cold cathode with an initial velocity $v_0 = 0$. Secondary electrons emitted from a cold cathode in low-voltage discharges are generally emitted at low energies. For example, the mean secondary electron energy is measured to be 6 eV for helium ions impinging on a tungsten cathode [15]. Starting the secondary electrons from the cold cathode at zero energy simplifies accounting procedures and should not seriously alter results. Subsequent to cold cathode secondary emission, the electrons gain energy as they are accelerated by the strong sheath field and lose energy through collisions.

IV. The Distribution in the Negative Glow

For the calculation of the bulk plasma electron energy distribution $N(E)$, one must consider the situation outside the sheath in the negative glow. As a first approximation, we assume that outside the cathode sheath the bulk plasma is field free and homogeneous. This does not necessarily contradict our assumption that 90 percent of the discharge voltage is dropped in the cathode sheath as the majority of the remaining drop occurs at the anode sheath and only a small percentage of the voltage is dropped in the negative glow region. Electrons launched from the sheath will lose energy in the bulk plasma via collisions and reach a steady-state distribution in energy. Under bulk plasma conditions, the Boltzmann equation (3) will simplify to the form

$$\vec{v} \cdot \nabla_r N(\vec{r}, \vec{v}) = \left(\frac{\delta N(\vec{r}, \vec{v})}{\delta t}\right)_c. \tag{5}$$

Using Gauss's theorem and integrating over full solid angles, the Boltzmann equation takes the simplified form

$$-S(E) = \left(\frac{\delta N(E)}{\delta t}\right)_c \tag{6}$$

where

$$S(E) = \frac{1}{V}\int_\Omega \oint_S v_n N(\vec{r}, \vec{v})\, dS\, d\Omega \tag{7}$$

and

$$N(E) = \frac{1}{V}\int_\Omega \int_{\vec{r}} N(\vec{r}, \vec{v})\, d^3\vec{r}\, d\Omega. \tag{8}$$

$S(E)$ represents the source flow of electrons into the bulk plasma. Solving (6) numerically within the bulk plasma, we obtain the electron energy distribution function $N(E)$. The electron flux density energy distribution at the sheath–bulk plasma interface is used as the source term $S(E)$ in (6).

V. Theoretical Energy Spectrum Results

The results of numerically solving (4) for the energy distribution of the electron flux at the sheath–glow interface are discussed below. The contribution of the various collision mechanisms to the electron energy spectrum are examined. To elucidate the relative role of the various collision mechanisms, the individual electron–atom collision processes are removed from the calculation one at a time. The collision processes are removed by making the cross section for that process equal to zero. As a result, as different processes are removed, the physical structure of the discharge can be strongly altered. That is, the reaching distance of electrons increases as the total cross section is reduced. A result of this is a larger sheath dimension and significantly modified current and voltage characteristics of the discharge. We have neglected these effects in this work, however, in an effort to provide a qualitative understanding of the roles of the various collision mechanisms in forming the shape of the electron energy distribution. As a result of our assumptions, many of the results presented are impossible to compare quantitatively, but shed much light on the effects of the electron collision mechanisms in shaping the electron energy distribution in the negative glow. The changing $I(E)$ spectrum provides a clear view of the effects of each type of collision.

Fig. 5(a) is a plot of the calculated electron energy spectrum at the sheath–glow interface with all the collision processes included. All calculations were made for an ambient helium pressure of 15 torr. There are six identifiable peaks in the theoretical spectra of Fig. 5(a) labeled *A*–*F*. Below we will examine the relative role of elastic, inelastic–excitation, and inelastic–ionization collisions in the formation of the electron flux peak structure. Controlled manipulation of the collision mechanisms included in the computer model allows the study of the effects of each of these mechanisms on the flux spectrum structure.

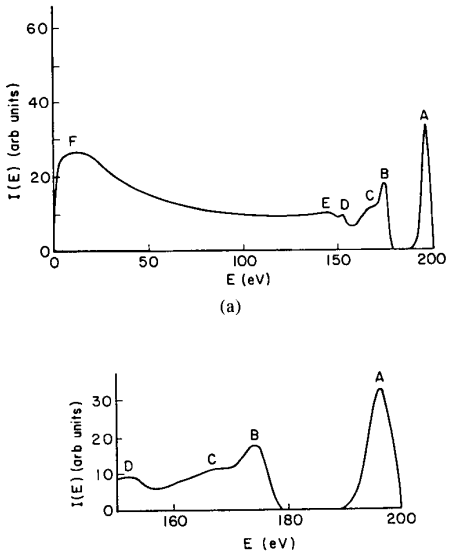

Fig. 5. Calculated electron energy distribution at the sheath–negative glow interface. (a) Full energy range. (b) Expanded view of the high-energy region.

An expanded view of the high-energy region of the distribution is shown in Fig. 5(b) for comparison to experimental results given later in this section.

Fig. 6(a) shows the calculated $I(E)$ distribution with inelastic collisions yielding excited helium atoms removed. In this instance, only three of the original peaks *A*, *C*, and *E* are evident in the high-energy region of the spectrum. Peak *C* is attributed to an electron having undergone one ionization collision during its acceleration through the sheath and peak *E* arises from two ionization collisions. The interval between the peaks *A* and *C* in the calculated spectra of Fig. 6(a) is larger than the separation between *A* and *B* in Fig. 5(a) because the peaks in Fig. 6(a) arise only from ionization collisions which have a characteristic 25 eV energy loss as compared to excitation collisions which have a lower threshold energy.

The calculated flux density distribution excluding only ionization collisions is given in Fig. 6(b). The observed peaks include *A*, *B*, and *D* which can arise only from excitation collisions. Peak *B* is due to a single excitation collision, and peak *D* represents two excitation collisions that occur during the electron flight through the sheath. Note the absence of the continuous distribution of electrons in the mid- to low-energy range as no secondary electrons are created at these energies due to the lack of ionization. For the same reason, the total number of electrons under the curves in Fig. 6(a) and (b) are not equal.

Fig. 7 illustrates the results of calculating the electron flux density energy distribution with ionization and excitation collisions included, but with all secondary electrons ejected from ionization collisions confined to zero energy and omitted from the distribution. All peaks in the spectrum are smoothed and broadened about 5 eV when compared to the spectra in Fig. 6(b) as the excitation and

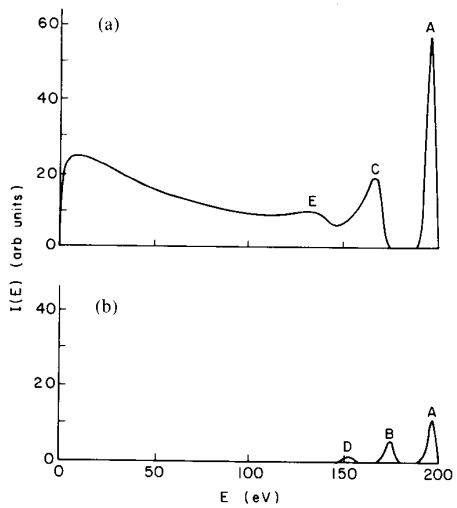

Fig. 6. Calculated electron energy distribution. (a) No excitation collisions. (b) No ionization collisions.

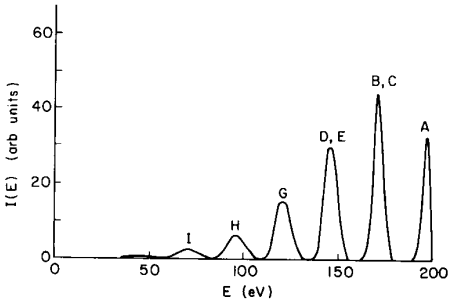

Fig. 7. Calculated electron energy distribution with secondary electrons confined to zero energy and omitted.

ionization peaks are now overlapping with a small offset (-5 eV) due to the different threshold energies for the two processes. The number of peaks in the spectrum of Fig. 7 is larger than the number in Fig. 6(b). Peaks G, H, and I arise from three, four, and five ionization events, respectively. The scale of the vertical axis has been changed in Fig. 7 to show the small peaks clearly.

Elastic collisions broaden and slightly shift the spectrum because of the very small energy change that occurs per elastic event, on the order of $(2m/M)E$ or $\sim 10^{-3}E$ for helium. Here, m is the electron mass, M is the helium atom mass, and E is the energy of the colliding electron. The spectrum obtained neglecting all elastic collisions but with both ionization and inelastic collisions maintained is given in Fig. 8. The comparison between Fig. 5(a) and Fig. 8 indeed confirms that elastic collisions not only smooth and broaden the peaks, but also slightly shift the peaks downwards in energy.

In addition to the six major peaks in Fig. 5(a), there is a single major minima that occurs in the spectrum. If we consider that no collisions of any type occur in the sheath, then $I(E)$ will be a delta function with a single peak at $E = eV_c$. If we include the possibility of elastic electron–atom collisions, then the single peak A will be both

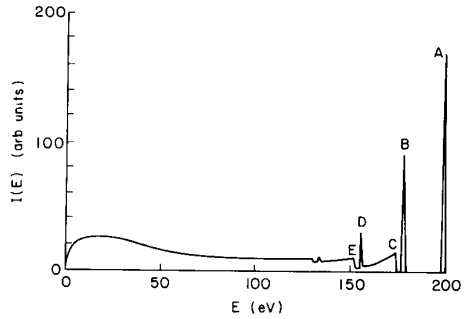

Fig. 8. Calculated electron energy distribution without elastic collisions.

broadened and shifted downwards toward lower energy. When inelastic–excitation collisions are included together with elastic collisions, several broad peaks will appear separated from each other by an energy characteristic of the spacing between the ground state and excited states. Inclusion of ionization collisions fills in the spectrum. Only the vacant space between peaks A and B arising from a single inelastic–excitation collision in the sheath is still present in Fig. 5(a) because no inelastic electron–atom collision can fill this gap.

Fig. 5(b) is an expanded view of the high-energy region of the distribution. Excellent agreement in the shape of the calculated and experimental (Fig. 1) distributions is observed within the high-energy portion of the spectrum. A gap of approximately 20 eV appears in both the calculated and experimental distributions.

There are some differences between the two distributions in Fig. 1 and Fig. 5(a) which occurs at low electron energies. The ratio of the relative heights of the low-energy peak F to the high-energy peak A in the theoretical distribution of Fig. 5(a) is smaller than the experimental peak ratio of Fig. 1. Reference [1] indicates that at low electron energies (less than 25 eV), a background "plasma" component is also included in the experimental data. This constitutes a large fraction of the total electrons in the low-energy portion of the experimental distribution. Up to this point, the plasma component has not been included in the theoretical calculation of Fig. 5(a), and thus there appear to be fewer electrons at low energies in the theoretical curve than in the experimental one. In the measurement apparatus of [1], the beam acceptance angle α is about 2.5°. The relationship between electron density $N(E)$ and electron flux density $I(E)$ into a small solid angle is found to vary as [16]

$$I(E) = AN_e\sqrt{\frac{2}{m}}\left(\frac{\sin\ \alpha}{2}\right)^2 N(E)\ \sqrt{E}. \qquad (9)$$

It must be emphasized that the spectrum being considered is only that portion of the plasma electrons which reach the experimental collector. A is the collector orifice area, N_E is the electron density, and m is the electron mass. The results of formula (9) were added to the results of Fig. 5(a) to achieve the calculated combined energy spectrum of Fig. 9. It is very similar to the one obtained by exper-

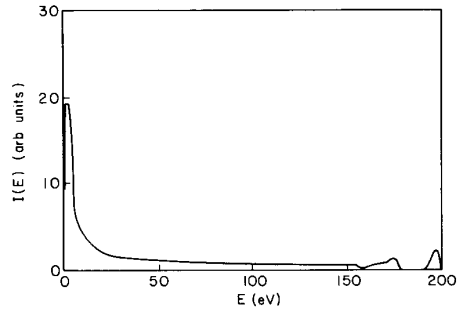

Fig. 9. The bulk plasma theoretical electron energy spectrum in a 15 torr He ambient.

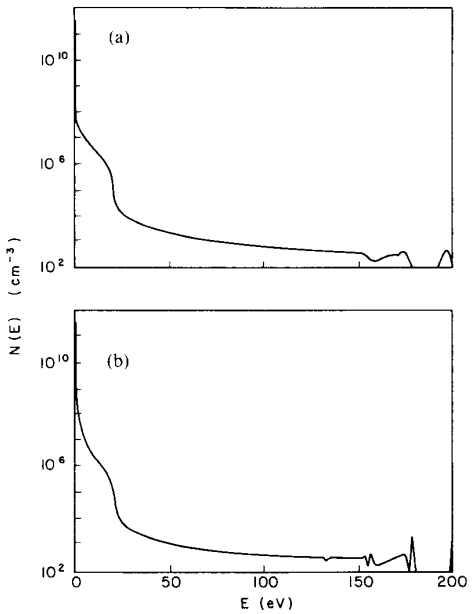

Fig. 10. Energy distribution of electron density in the bulk plasma (a) using $S(E)$ from Fig. 5(a), (b) using a delta function input from the sheath for $S(E)$.

iment as shown in Fig. 1. The abundance of low-energy electrons in the plasma arises from ejected secondary electrons created by ionization collisions.

The result of solving (6) for the bulk plasma electron energy distribution is given in Fig. 10(a). There is a high-energy peak component as obtained previously in Fig. 5(a), but its peak height is much smaller than the peak located at low energies. For comparison, Fig. 10(b) gives the electron energy distribution obtained if a delta function approximation is used as the source term of electrons launched into the bulk plasma. The delta function source term gives a sharply varying high-energy tail in $N(E)$ which is quite different from the smoothly varying experimental one shown in Fig. 1. Note that the low-energy portions of Fig. 10(a) and (b) are roughly the same despite the different source term choices.

To allow our results to be compared to the experimental results of Olson and Nordlund [6], we have plotted the normalized electron energy distribution in the negative

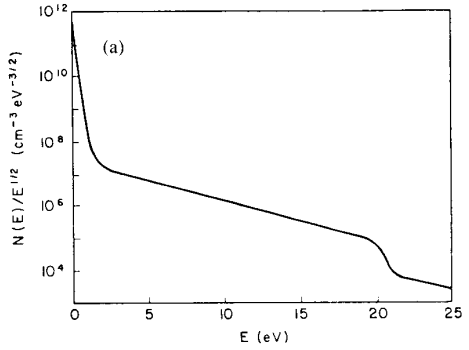

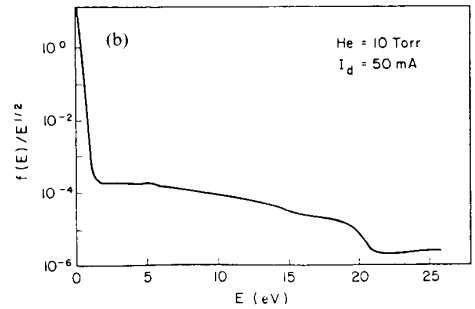

Fig. 11. Expanded view of the low-energy portion of Fig. 10(a). (b) Olson and Nordlund's measurement of the bulk plasma electron distribution $N(E)$.

glow region of the discharge in Fig. 11(a). For comparison, the results of Olson and Nordlund are shown in Fig. 11(b). Good qualitative agreement is observed in the shape of Fig. 11(a) and (b). The sudden drop at 20 eV in Fig. 11(a) and (b) arises mainly due to the energy threshold for the excitation cross sections.

VI. Conclusions

Good qualitative agreement between theoretical and experimental electron energy distributions is found over a wide energy range. The unique effects of inelastic and elastic collision mechanisms have been elucidated. The results of the calculations indicate that the shape of the electron energy distribution in the bulk plasma is strongly influenced by the effects of electron collisions in the sheath region of the discharge.

The effects of ionization collisions dominate the structure of the distribution both inside the cathode sheath and in the bulk plasma region. Ionization collisions are responsible for several of the peaks observed in the high-energy region of the distribution, the smooth midenergy region, as well as a portion of the large "thermal" component of the distribution. Secondary electrons emitted in ionization events are also responsible for smoothing the $I(E)$ distribution. Excitation collisions are responsible for several peaks in the high-energy region of the distribution, but their effects on $I(E)$ are overwhelmed by the smoothing effect of the secondary electrons emitted in ionization events. The role of elastic collisions is seen to

be important to $I(E)$, primarily at low energies in this type of discharge.

ACKNOWLEDGMENT

Special thanks are due to Prof. M. Kushner and Dr. B. Warner for their detailed corrections to the draft manuscript and their suggestions for improvements.

REFERENCES

[1] P. Gill and C. E. Webb, *J. Phys. D*, vol. 10, p. 299, 1977.
[2] S. C. Brown, *Basic Data of Plasma Physics*. Cambridge, MA: M.I.T. Press, 1959, p. 281.
[3] B. E. Warner, Ph.D. dissertation, Dep. Phys., Univ. Colorado, Boulder, 1979.
[4] G. J. Fetzer, J. J. Rocca, G. J. Collins, and R. Jacobs, *J. Appl. Phys.*, vol. 60, p. 2739, 1986. See also, T. J. Sommerer, J. E. Lawler, and W. Hitchon, *J. Appl. Phys.*, vol. 64, p. 1775, 1988.
[5] W. D. Davis and T. A. Vanderslice, *Phys. Rev.*, vol. 131, p. 219, 1963.
[6] R. A. Olson and D. R. Nordlund, Wright-Patterson AFB, OH, Tech. Rep. AFAL-TR-73-420, 1973.
[7] J. R. McNeil, Ph.D. dissertation, Colorado State Univ., Fort Collins, 1979.
[8] R. K. Janev, W. D. Langer, K. Evans, Jr., and D. E. Post, "Atomic and molecular processes in hydrogen-helium plasmas," Plasma Phys. Lab., Princeton Univ., Princeton, NJ, June 1985.
[9] S. Moriya, P. Zeller, and G. J. Collins, presented at the 40th Gaseous Electron. Conf., Atlanta, GA, Oct. 1987.
[10] B. Shi, J. Meyer, Z. Yu, and G. J. Collins, *IEEE Trans. Plasma Sci.*, vol. PS-14, p. 523, 1986. See also, R. J. Carman and A. Maitland, *J. Phys. D*, vol. 20, p. 1021, 1987.
[11] H. S. W. Massey, E. H. S. Burhop, and H. B. Gilbody, *Electron and Ionic Impact Phenomena*. Oxford: Clarendon, 1969.
[12] C. B. Opal, *Atomic Data*, vol. 4, p. 209, 1972.
[13] J. Bretagne, G. Delouya, J. Godart, and V. Puech, *J. Phys. D.*, vol. 14, p. 1225, 1981.
[14] A. Von Engle, *Ionized Gases*. Oxford: Clarendon, 1955; See also, T. J. Sommerer, J. E. Lawler, and W. N. G. Hitchon, *J. Appl. Phys.*, vol. 64, no. 4, p. 1775, 1988.
[15] M. Kaminsky, *Atomic and Ionic Impact Phenomena on Metal Surfaces*. New York: Academic, 1965, p. 291.
[16] R. Boyd and F. Boylett, *Proc. Roy. Soc.*, vol. A296, p. 233, 1966.

B. Shi, photograph and biography not available at the time of publication.

G. J. Fetzer, photograph and biography not available at the time of publication.

Z. Yu, photograph and biography not available at the time of publication.

J. D. Meyer (S'83-M'83-S'84-M'86), photograph and biography not available at the time of publication.

G. J. Collins (S'62-S'69-M'72-SM'75-F'87), photograph and biography not available at the time of publication.